Variable magnetic field technology and permanent magnet characteristic by the request of electric traction motors

H. Nakai*

(Toyota Central R&D Labs., Inc.)

A traction electric motor of HV, PHV and EV is required high efficiency to reduce fuel consumption. While, to secure passengers space, the motor is also demanded downsizing. Since the motor is in the industrial products, low-cost is also required without doubt. The motor requests a several characteristic of a permanent magnet for fulfilling above 3 demands. In order to downsize the motor, firstly, we need a high magnetic flux density magnet (a strong magnet) and a magnet which is hard to demagnetize. The motor is often put in a small space for which it is easy to be filled with heat, for example, an engine compartment. The motor which uses a strong magnet can produce large torque, even though the motor is put in a small space. The motor is often cooled using by a transmission fluid to prevent temperature rise. Even if the motor is chilled using the fluid, the temperature is more than 100℃. Therefore, the magnet which is hard to demagnetize in high temperature is desired in the motor. Almost traction motors use a Nd-Fe-B sintered permanent magnet in order to fulfil the demand of minimization and demagnetization. It is, however, a problem that the Nd-Fe-B magnet has high cost price. Reducing the cost of the Nd-Fe-B magnet is a 2nd request of the motor. In order to realize high efficiency which is a 3rd demand for the motor, we request high electrical resistance magnet and variable magnetic field magnet. Cyclical change of magnetic resistance caused by stator tooth make a magnetic flux change in a magnet placed in the motor. An eddy current occurred by the magnetic flux change makes loss in a magnet. High electrical resistance of a magnet avoids eddy current and reduces the loss. Reduction of the loss achieves increasing motor efficiency. Maximum torque of the motor determines a magnet force in many situations. However, the magnet force is often too strong to achieve high efficiency in high rotational speed and small load area. The efficiency in this area has great influence on fuel consumption of a vehicle. Therefore, variable magnetic field magnet is desired to improve efficiency. The strength of a Nd-Fe-B magnet is also fixed like other permanent magnets. The motor used in vehicle replaces a part of magnet torque with reluctance torque to carry out variable magnetic field. Reluctance torque is not, however, large enough to replace all magnet torque. So, last 10 years several studies which achieve variable magnetic field using not only reluctance torque but also new mechanisms have been done actively. As one kind of studies which achieve variable magnetic field, there is a motor which controls permanent magnetic force[1]. The advantage of this motor is that the structure is almost same with an ordinary IPM motor. The disadvantage is vibration occurred by pulse current which is used for controlling magnet force. Changing magnetic resistance method using mechanical way[2] is one of a variable magnetic field study. The advantage of this method is that the magnetic field can be accurately measured using a mechanical air-gap. The motor needs, however, a mechanical actuator. This actuator is a weak point. Other method controlling magnetic force has an electromagnet in addition to a permanent magnet. This method has ability changing magnetic force quickly because of an electromagnet. An electromagnet needs space bigger than a permanent magnet. Therefore, it is a problem to increase the size of the motor. There is a study solving this problem in order to achieve downsizing with high efficiency[3]. The proposed motor in Fig. 1 constitutes a 3-DOF magnetic circuit with dust core. The circuit has one radial air-gap and two axial air-gaps to increase torque density. This motor settles an excited field coil of an electromagnet in the gap of a radial and an axial air-gap not to increase the size. Therefore, this motor can achieve variable magnetic field with downsizing. As mentioned as above, traction motor demands various performances to a magnet. A magnet that satisfies all performance has not yet been developed. Development of a higher-performance magnet will improve characteristic of the motor and realize restraint of the global warming.

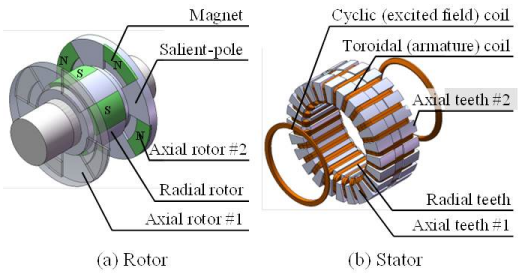

Fig. 1　3 air-gaps motor with excited field coils.

References

1) K. Sakai et al., *IEEJ Transactions on Industry applications*, **Vol.131**, **No.1**, pp.53-60 (2011) (in Japanese).
2) H. Nakai et al., *JIASC2007*, **No.3-64**, pp.337-342 (2007) (in Japanese).
3) M. Namba et al., *IEEJ Transactions on Industry applications*, **Vol.135**, **No.11**, pp.1085-1090 (2015) (in Japanese).

Development of Measurement Technique of Three-dimensional Demagnetization Distribution in Permanent Magnets for Motors

Y. Asano, S. Araki, A. Yamagiwa
(Technology Research Association of Magnetic Materials for High-Efficiency Motors (MagHEM))

It is important to estimate the demagnetization state in the magnets in Interior Permanent Magnet Synchronous Motors (IPMSMs), which are often used for consumer electronics and HEV traction motors . However, the distribution of demagnetization in permanent magnets for these motors is not uniform due to the difference of coercivity of local parts in the magnet material and the difference of the working point of local parts in the magnet caused by the variation of magnetic circuit in a motor. So, it was necessary to estimate the demagnetization distribution in the magnet by FEA, because there were not techniques to measure that. Therefore, we develop a method to evaluate the three-dimensional demagnetization state including the inside the magnet by cutting the magnet into the cubes, as shown in Fig. 1, and measuring the B–H characteristics of each magnet cube using Vibrating Sample Magnetometers (VSM), as shown in Fig. 2. At first we lock the motor rotation in high temperature environment, and an electric current is applied into a coil to hang opposing magnetic field. Next, magnets are taken out from the motor. Then, we cut the magnet into the cubes without demagnetizing anymore. Finally, we measure the B–H characteristics of each magnet cube shown as in Fig. 3 and , formula[1] and calculate demagnetizing ratio distribution.

$$\text{Demagnetizing ratio}[\%]=(B1-B2)/B1\times 100 \quad [1]$$

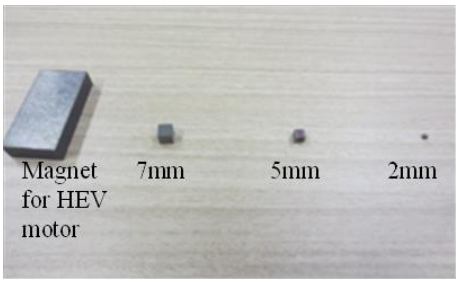

Fig.1. Magnet cut into cubes

Fig. 2. Vibrating Sample Magnetometers VSM

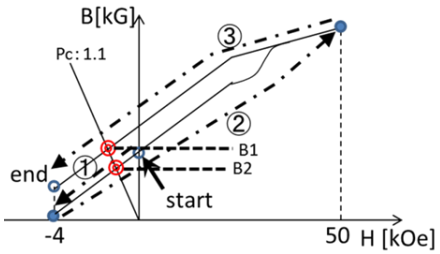

Fig.3. Calculation method of demagnetizing ratio

Reference

1) S. Araki, Y. Asano, A. Yamagiwa, “Development of Measurement Technique of Three-dimensional Demagnetization Distribution in Permanent Magnets for Motors (Part 1)” The paper of joint Technical Meeting on Rotating Machinery, Linear Drive and Home and Consumer Appliances, IEE Japan, RM-15-083/LD-15-034/HCA-15-036(2015)

Grain size refinement of Nd-Fe-B sintered magnets

Y. Une, H. Kubo, T. Mizoguchi, T. Iriyama and M. Sagawa

(Intermetallics Co., Ltd. (Technology Research Association of Magnetic Materials for High-Efficiency Motors / Nagoya Branch), Creation-Core Nagoya 101, 2266-22 Anagahora, Shimo-shidami, Moriyama-ku, Nagoya, Aichi 463-0003, Japan)

High remanence and large coercivity are required for Nd-Fe-B magnets in high-efficiency motors such as traction motors for EV or HEV. The addition of Dy is the most common way to increase the coercivity of Nd-Fe-B magnets. The problem of the Dy addition is the reduction of the remanence or the rise of material cost. Accordingly, efforts to reduce Dy use have been undertaken all over the world. One of the important idea to reduce the Dy use is a grain size refinement of $Nd_2Fe_{14}B$ crystal. Also, optimizing the grain boundary structure is necessary to achieve the large coercivity. We have been challenging the grain size refinement of Nd-Fe-B sintered magnets since 2007.

From 2007 to 2012, we had developed under “Rare Metal Substitute Materials Development Project” commissioned by the New Energy and Industrial Technology Development Organization (NEDO). In this project, we obtained fine powder with average particle size of around 1 μm using a helium jet-milling[1]. We fabricated the fine grained Dy-free Nd-Fe-B magnets using this powder with coercivity of around 20 kOe; about 40% of Dy can be saved by this technique.

Then, from 2012 to now, we have been challenging to develop the new production process for the further grain size refined Dy-free Nd-Fe-B sintered magnets under "Future Pioneering Projects / Development of magnetic material technology for high-efficiency motors" commissioned by NEDO.

The sub-micron grained sintered magnet was developed using both HDDR process and helium gas jet-milling[2]. This magnet (HDDR sintered magnet) had a better temperature coefficient of coercivity than the conventional sintered magnet. However, the coercivity at room temperature is around 13 kOe which is rather lower than we expected[3]. It can be seen that the HDDR sintered magnet has thinner Nd-rich grain boundary phase with around 1 nm than that of conventional magnet (thickness: 2 nm). We have been trying to expand the grain boundary phase of the HDDR sintered magnets by various methods such as the grain boundary diffusion (GBD) technique. One of the results is shown in Fig.1.

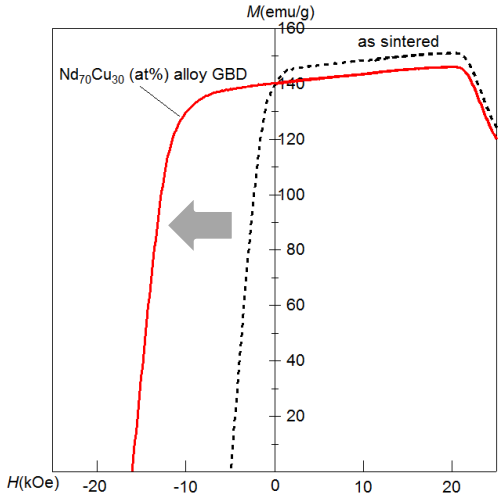

Fig.1 GBD for the HDDR sintered magnets

References

1) Y. Une and M. Sagawa, J. Jpn. Inst. Met. **76**, 12 (2012) (in Japanese)
2) M. Nakamura, M. Matsuura, N. Tezuka, S. Sugimoto, Y. Une, H. Kubo, and M. Sagawa, Appl. Phys. Lett. 103 (2013) 022404.
3) Y. Une, H. Kubo, T. Mizoguchi, T. Iriyama, M. Sagawa, M. Nakamura, M. Matsuura, and S. Sugimoto, The 38th Annual Conference on MAGNETICS in Japan (2014), 2pB-2

Newly developed $(R,Zr)(Fe,Co)_{12-x}Ti_x$-N_y compounds for permanent magnets (y=1.3 for R=Nd, y=0 for R=Sm)

K. Kobayashi, S. Suzuki, T. Kuno and K. Urushibata
(Shizuoka Institute of Science and Technology, Toyosawa 2200-2, Fukuroi, Shizuoka 437-8555, Japan)

$(R_{0.7\text{-}0.8}Zr_{0.3\text{-}0.2})(Fe_{0.75}Co_{0.25})_{11.5}Ti_{0.5}$ (R = Nd and Sm) alloys for permanent magnet materials were prepared by strip-casting. The homogeneity of the elements detected using electron-probe micro-analysis (EPMA) was fairly good. The occupation sites of the substituted elements, i.e. Zr in R sites, Ti in Fe(8i) sites and Co in Fe(8j) and Fe(8f) sites, were revealed by using spherical aberration-corrected scanning transmission electron microscopy (Cs-STEM). The stabilization of $ThMn_{12}$ structure at a low Ti content of $Ti_{0.5}$ mainly originated from the substitution of R sites with Zr. The nitrogenated R = Nd alloy, $(Nd_{0.7}Zr_{0.3})(Fe_{0.75}Co_{0.25})_{11.5}Ti_{0.5}N_{1.30}$ compound, showed good magnetic properties of J_s = 1.67 T and H_a = 5.25 MA/m at room temperature (RT). The R = Sm alloy, $(Sm_{0.8}Zr_{0.2})(Fe_{0.75}Co_{0.25})_{11.5}Ti_{0.5}$, also had J_s = 1.58 T and H_a = 5.90 MA/m at RT. The values in the R = Sm alloy were still J_s = 1.50 T and H_a = 3.70 MA/m at 473 K, and were higher than those of $Nd_2Fe_{14}B$ phase at the temperature [1]-[6]. Because the R = Sm alloy is a Dy-free and N-free powder, it is a promising candidate as a material for sintered magnets (4).

For the measurement of magnetic properties of the samples, physical properties measurement system-vibrating sample magnetometer (PPMS-VSM) under a maximum applied field of 9 T was employed. Especially, the J_s and H_a, i.e. K_1, was calculated from the magnetization curve using the law of approach to saturation (LAS) method. The sample powder consisted of secondary grains composed of isotropic agglomerated primary grains of about 5×5~20 μm. The sample powder was mixed in epoxy resin, then the magnetically isotropic sample. The analysis was performed by using the following equation [7], [8].

$$dJ(H) / dH = J_S (8/15) (K_1^2/J_S^2) (1/H^3)) + \chi_0 \qquad (1)$$

Here, $J(H)$ is the measured polarization under applied field H, J_S is the saturation polarization, and K_1 is the first-order anisotropy constant. Equation (1) was applied to the measured polarization under a high field of 6-9 T, and the plots between $dJ(H)/dH$ and $1/H^3$ are used to calculate J_S and K_1 values. This method was used to obtain the results in our previous studies [1]-[4] . In the study [4] , however, we compared the results obtained using above equation (1) with those using $J(H)$ vs $1/H^2$ plots, and employed the latter method for the stability of obtained values. As mentioned above, the comparatively high magnetic properties in R=Nd nitrogenated compound and R=Sm alloy were measured using the LAS method.

Evaluating the α-(Fe,Co) phase concentrations in the samples is important for calculating precise J_s. We determined the volume fractions of the phase using two methods. First, we compared the largest XRD peak height of the α-(Fe,Co) phase around 2θ=44.5º with that of the main $ThMn_{12}$ phase of around 2θ=42.4º. The ratios of peak heights corresponded to the volume fractions of the phases. This method included the error from the crystallinity of each phase in the samples and the local distribution of the phases in the sample particles. Second, we obtained the volume fractions directly, through measuring the surface area fractions of the α-(Fe,Co) phase on the polished surface of electron back-scattering diffraction (EBSD) image of the sample particles. Each phase was clearly distinguished in this method, however, there were errors arising from the difference in the particles observed. Although numerous observations are required for this method, the number of observations was limited for some particles in the experiments.

The above J_S values of samples were corrected using XRD data those for eliminating the contribution from α-(Fe,Co) phases. The obtained values were indicated in Fig.1. The values (a) were shown in our previous papers [1]-[4], and those of (b) were newly obtained in our recent measurements.

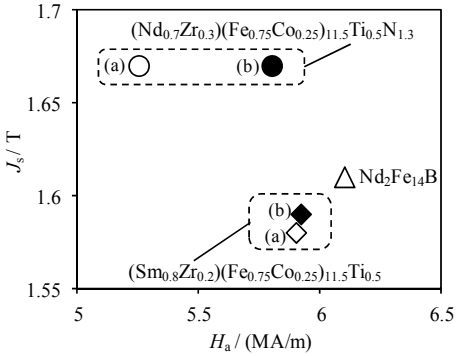

Fig. 1 Results of the LAS method using PPMS-VSM (at RT)

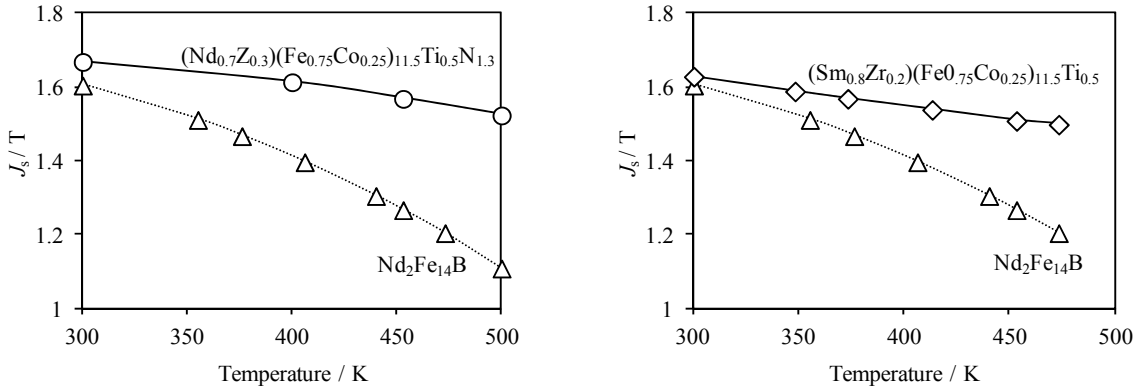

Fig. 2 Temperature dependences of J_s in R=Nd compound (a) and in R=Sm alloy (b) with those in $Nd_2Fe_{14}B$ phase [6].

The Curie temperature (T_c) of the alloys was measured also using the PPMS-VSM with an maximum applied field of about 9 T. *T*c of $(Nd_{0.7}Zr_{0.3})(Fe_{0.75}Co_{0.25})_{11.5}Ti_{0.5}N_{1.30}$ compound is more than 840K that is sufficiently higher than that of an Nd-Fe-B magnet of about 584 K [5], [6]. The temperature dependences of J_s (Fig. 2) and H_a of the alloys showed that the J_s and H_a values at 473 K of $(Nd_{0.7}Zr_{0.3})(Fe_{0.75}Co_{0.25})_{11.5}Ti_{0.5}N_{1.30}$ compound and $(Sm_{0.8}Zr_{0.2})(Fe_{0.75}Co_{0.25})_{11.5}Ti_{0.5}$ alloy (T_C estimated to be 880K) were higher than those of Nd-Fe-B (the figure for H_a exists in ref.[4]). As mentioned above, $(Sm_{0.8}Zr_{0.2})(Fe_{0.75}Co_{0.25})_{11.5}Ti_{0.5}$ has still J_s = 1.50 T and H_a = 3.70 MA/m at 473K, and we would like to insist again that the alloy is Dy-free and N-free, therefore, it is a promising candidate for permanent magnet material for high-temperature applications.

Acknowledgement

This report is based on results obtained from the pioneering program “Development of magnetic material technology for high-efficiency motors” (2012–) commissioned by the New Energy and Industrial Technology Development Organization (NEDO).

References

[1] S. Suzuki, T. Kuno, K. Urushibata, K. Kobayashi, N. Sakuma, K. Washio, M. Yano, A. Kato, A. Manabe, J. Magn. Magn. Mater. vol.401 (2016) p.259-268.

[2] S. Suzuki, T. Kuno, K. Urushibata, K. Kobayashi, N. Sakuma, K. Washio, H. Kishimoto, A. Kato and A. Manabe, AIP Advances 4 (2014) 117131.

[3] N. Sakuma, S. Suzuki, T. Kuno, K. Urushibata, K. Kobayashi, M. Yano, A. Kato and A. Manabe, AIP Advances 6 (2016) 056023.

[4] T. Kuno, S. Suzuki, K. Urushibata, K. Kobayashi, N. Sakuma, M. Yano, A. Kato and A. Manabe, AIP Advances 6 (2016) 025221.

[5] M. Sagawa, S. Fujimura, N. Togawa, H. Yamamoto, and Y. Matsuura, J. Appl. Phys. 55 No.6 (1984) p.2083-2087.

[6] S. Hock, Ph.D. thesis, Ph.D thesis, Universität Stuttgart (1988).

[7] H. Kronmüller and M. Fähnle, Micromagnetism and the Microstructure of Ferromagnetic Solids, Cambridge (2003) p.174.

[8] G. Hadjipanayis, D.J. Sellmyer, and B. Brandt, Phys Rev., B 23 No.7 (1981) p.3349-3354.

Research trends for the high-performance La-Co substituted M type ferrite magnets

Yoshinori Kobayashi
Hitachi Metals, Ltd.

1. Introduction

The hexagonal Sr-M type ferrite magnet has been widely used in applications such as the motor for car electrical equipments and for air conditioners and refrigerators. Recently, the magnetic properties of ferrite magnet has been improved by substituting La and Co for Sr and Fe atoms, respectively. The La-Co substituted M-type ferrites (Sr-La-Co M-type ferrite and Ca-La-Co M-type ferrite, to which we will refer as 'SLC-M' and 'CLC-M' hereafter)[1)-3)] are known to have the higher magnetic crystalline anisotropy compared with Sr-M type ferrite. In this study, the occupation sites of cobalt ions in the La-Co substituted M-type ferrite compound were analyzed by the neutron diffraction, the extended X-ray absorption fine structure (EXAFS) and the X-ray magnetic circular dichroism (XMCD) to understand the relationship between the local structure and the improvements of magnetic characteristics in the La-Co substituted M-type ferrite, and furthermore, microstructure of CLC-M sintered ferrite magnets were analyzed by Spherical Aberration Corrected Scanning Transmission Electron Microscopy (Cs-STEM) to get guiding principles for improving magnetic property.

2. Cation distribution analysis of La-Co M-type ferrites by neutron diffraction, EXAFS and XMCD[4), 5)]

We investigated the site distribution of the cobalt ions in SLC-M ($Sr_{0.7}La_{0.3}Co_{0.3}Fe_{11.3}O_{19}$) and CLC-M ($Ca_{0.5}La_{0.5}Co_{0.3}Fe_{10.1}O_a$, a≈19) by neutron diffraction and EXAFS measurements. Fig. 1 shows the one half of unit cell for Sr-M ($SrFe_{12}O_{19}$, space group: $P6_3/mmc$). The five different sublattices for the ferric ions are denoted using Wyckoff's notation as follows: 12k, 2a, $4f_2$ (octahedral sites), $4f_1$ (tetrahedral site) and 2b (bipyramidal site). In this study, we estimated the local structure on the assumption that cobalt ions simultaneously occupy some of the five ferric ion sites. It was suggested that cobalt ions are partitioned in the 2a, $4f_1$ and 12k sites in the ratio of 1:2:2 for SLC-M. Meanwhile, it was suggested that cobalt ions are partitioned in the 2a, $4f_1$ and 12k sites in the ratio of 2:6:2 for CLC-M.

Fig. 2 shows the X-ray absorption near edge structure (XANES) spectra and the XMCD spectra at the Fe *K*-edge for Sr-M, SLC-M and CLC-M. The ferric ions at the tetrahedral site (A site) of the spinel ferrite give a pre-edge peak around *E*≈7.11 keV in the XANES spectrum[6)]. The pre-edge peak is observed in the XANES spectra at the Fe *K*-edge for Sr-M, SLC-M and CLC-M. The M type ferrite has a ferrimagnetic structure, that is, eight ferric ions with the up-spin at 2a, 2b, 12k and four ferric ions with the down-spin at $4f_1$, $4f_2$ exist in a unit cell. The pre-edge peak originates from the ferric ions of the down spin at the tetrahedral site, $4f_1$. The intensity of the XMCD spectrum peak at the pre-edge peak is smaller for CLC-M than for Sr-M and SLC-M. This suggests that the contributions of the ferric ions in the down spin site to a magnetic moment decreases, suggesting that the ferric ions at the tetrahedral site $4f_1$ is replaced by more elements of a smaller or no magnetic moment for CLC-M compared to Sr-M and SLC-M.

3. Microstructural analysis of Ca-La-Co M-type sintered ferrite magnets by Cs-STEM[7)]

We investigated composition and microstructure at the vicinity of grain boundary by Cs-STEM for CLC-M sintered body. Table 1 shows EDX analysis results for multiple-junction phases of CLC-M sintered body with additives : (a) $CaCO_3$:0.0 mass%, SiO_2:0.34 mass%, (b) $CaCO_3$:1.25 mass%, SiO_2:0.68 mass%. It was confirmed that there are Ca-Si based oxides, which consists of Si, Ca, La and Fe, at multiple-junction phases of sintered body by adding only SiO_2 instead of both $CaCO_3$ and SiO_2 which are sintering aids for ferrite magnets. And then it was almost confirmed that the abundance ratio of Si, Ca, La and Fe at multiple-junction phases is 30：60：2：5.

Fig. 3 shows HAADF-STEM image on intergranular grain boundary for CLC-M sintered body with additives : $CaCO_3$:1.25 mass%, SiO_2:0.68 mass%. We found that the step-terrace structure of Ca-Si based oxides are formed at the surface of the M-type ferrite grain, and the maximum width of intergranular grain boundary is nearly equal to half the edge length along z-axis, which is 1.15 nm, of M-type ferrite unit cell. This suggests that M-type ferrite grains were magnetically isolated by the presence of Ca-Si based oxide phases at intergranular grain boundary.

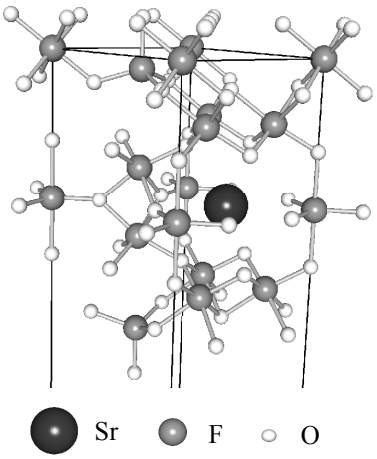

Fig.1 One half of unit cell of the Sr-M type hexaferrite ($SrFe_{12}O_{19}$, space group: $P6_3/mmc$).

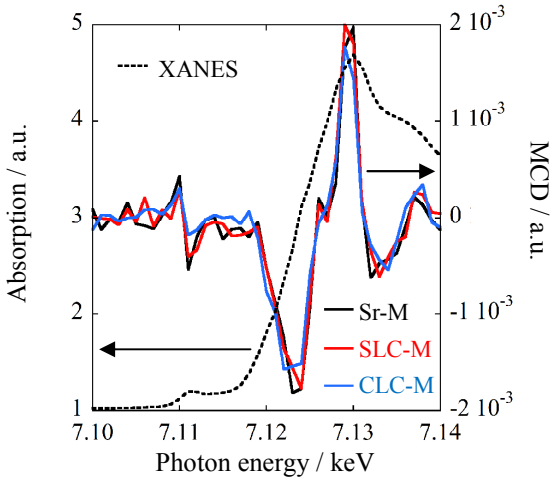

Fig. 2 The XANES and hard X-ray MCD spectra for the Sr-M and the La-Co substituted M type ferrite.

Table 1 EDX analysis results for multiple-junction phases of CLC-M sintered body with additives.

(a) $CaCO_3$:0.0 mass%, SiO_2:0.34 mass%

	Si (at%)	Ca (at%)	La (at%)	Fe (at%)
1	29.3	64.1	2.7	3.9
2	27.7	67.2	1.6	3.5
3	32.4	60.2	2.0	5.4
4	29.7	60.4	3.3	6.6
5	30.9	63.9	1.3	3.9
Ave.	30.0	63.1	2.2	4.7

(b) $CaCO_3$:1.25 mass%, SiO_2:0.68 mass%

	Si (at%)	Ca (at%)	La (at%)	Fe (at%)
1	30.2	63.5	1.2	5.1
2	30.9	62.0	1.5	5.6
3	30.7	63.3	1.7	4.3
4	30.1	62.2	1.9	5.8
5	31.7	60.5	1.1	6.7
Ave.	30.7	62.3	1.5	5.5

Fig. 3 HAADF-STEM image on intergranular grain boundary for CLC-M sintered body with additives. ($CaCO_3$:1.25 mass%, SiO_2:0.68 mass%)

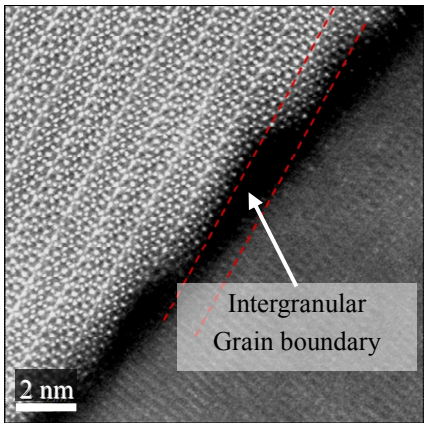

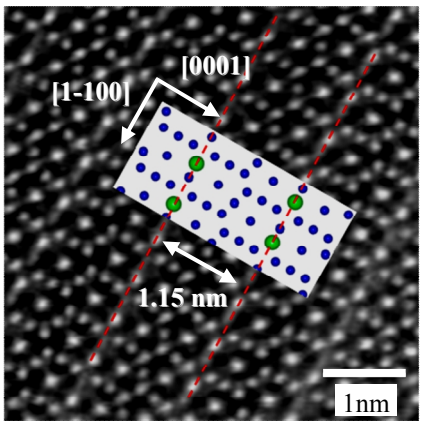

Reference

1) K. Iida, Y. Minachi, K. Masuzawa, J. Magn. Soc. Jpn., 23 (1999) 1093-1096.
2) H. Nishio, K. Iida, Y. Minachi, K. Masuzawa, M. Kawakami, H. Taguchi, J. Magn. Soc. Jpn., 23 (1999) 1097.
3) Y. Kobayashi, S. Hosokawa, E. Oda, S. Toyota, J. Jpn. Soc. Powder Powder Metallurgy, 55 (2008) 541.
4) Y. Kobayashi, E. Oda, T. Nishiuchi and T. Nakagawa, J. Ceram. Soc. Jpn., 119[4] (2011) 285.
5) Y. Kobayashi, E. Oda, T. Nakagawa and T. Nishiuchi, J. Jpn. Soc. Powder Powder Metallurgy, 63 (2016) 101.
6) N. Kawamura, Doctoral thesis, University of Okayama, Okayama, Japan, (1999) 88.
7) Y. Kobayashi, T. Kawata, submitted.

Observations of Coercivity in RE-Fe-B Magnets in Pulsed Fields up to 30T

K. Nakahata[1], K Yamada[2], H. Shimoji[3] and M. Enokizono[4]
[1]Oita Advance Technical Academy, Oita 870-1141, Japan
[2]Saitama University, Saitama 338-8570, Japan
[3]Oita Pref. Industrial Research Institute, Oita 870-1117, Japan,
[4]Oita University, Oita 870-1192, Japan

The measurements of the coercivity (*Hc*) of magnets are very important to obtain the stored energies in magnets. However it is difficult to determine *Hc* as a function of the effective fields in samples with arbitrary shapes in pulsed fields. We tried to obtain the exact coercive force and the *M-H* curve in high pulsed magnetic fields up to 30T with long pulsed fields (e.g. half width of 80ms in $20T_{max}$) by using an induction method with a triple-fold pick-up coil [1]. In this experiment, the values of *Hc* were found much smaller than *10-20*% in the Nd-Fe-B and in Sm-Fe-B magnets which were supplied and announced ratings by a company. These errors might be caused by the sample insertion gap in between the sample and probe. These magnetic field configurations of samples with some insertion gaps of the pick-up coil were well simulated using JMAG and were well coincide with the experimental results. Fig. 1 shows the experimental results of H_{eff} vs. $\mu_0 H$ for two samples of Nd-Fe-B. Table1 shows the discrepancies of the several parameters between the announced values and those in this study. Here it must be noted that we obtained the same samples with a sample maker and we prepared two types of samples which were cut along easy and hard axis, respectively. Therefore, to avoid errors, we prepared samples with the largest diameter up to the allowance to insert samples into the inner diameter of the pick -up coil (*10*mm$^{\Phi}$). The physical origin of this discrepancy is very plausible to consider the magnetic flux density at $B=\mu_0 H_{eff}+M$. In other words, at the coercive field (*Hc, M=0*), the effective fields as a function of the positions are uniform as described by $B= \mu_0 H_{eff} (=\mu_0 Hc)$. Therefore the voltages in the pick-up coil with its cross section are always larger than those of the samples by the insertion gap.

References

[1] K. Nakahata,B. Borkovsky, K. Yamada,T. Todaka, M. Enokizono, J. AEM,Vol.19,No2,pp207-212, ,2011

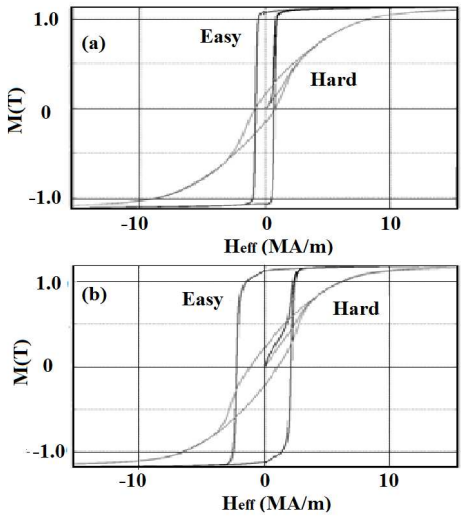

Fig.1 Experimental results of M-H curves of Nd-Fe-B magnets measured along Easy and Hard axes in pulsed fields

Table 1. Experimental results of typical samples

Nd-Fe-B(1)	Easy	Hard	Easy(Catalog)
Mr (T)	1.48	0.168	1.48
H_{cB}(kA/m)	867	91.1	1046
H_{cJ}(kA/m)	1024	607	875
$(BH)_{Max}$	314	3.90	421

Nd-Fe-B(2)	Easy	Hard	Easy(Catalog)
Mr (T)	1.12	0.16	1.13
H_{cB}(kA/m)	697.2	92.3	835 - 915
H_{cJ}(kA/m)	2499	1051	2387
$(BH)_{Max}$	197	3.76	240

Sm-Fe-B(c)	Easy	Hard	Easy(Catalog)
Mr (T)	1.07	0.16	1.08
H_{cB}(kA/m)	579	88.9	557
H_{cJ}(kA/m)	753	767	598
$(BH)_{Max}$	174.8	3.48	215